The final publication is available via Elsevier at https://doi.org/10.1016/j.culher.2019.04.005.

Please cite as: Lercari, N. 2019. Monitoring Earthen Archaeological Heritage using Multi-Temporal Terrestrial Laser Scanning and Surface Change Detection. *Journal of Cultural Heritage*, 2019. DOI 10.1016/j.culher.2019.04.005.

Monitoring Earthen Archaeological Heritage using Multi-Temporal Terrestrial Laser Scanning and Surface Change Detection

Corresponding author: Nicola Lercari

Affiliation: Department of Anthropology and Heritage Studies, University of California, Merced

Permanent Address: 5200 North Lake Road, 95343, Merced, CA (nlercari@ucmerced.edu)

Abstract

Terrestrial laser scanning (TLS) is a three-dimensional survey technique proven successful for in-field stratigraphic and site-wide documentation or damage assessment of archaeological heritage. This study explores the potential utility of TLS and the Multiscale Model to Model Cloud Comparison (M3C2) surface change detection method for monitoring and preserving ancient earthen architecture, and for creating comprehensive site monitoring programs in compliance with UNESCO periodic reporting guidelines. The proposed methodology was tested using 3-D TLS datasets spanning a period of six years to assess the decay of mud brick structures at Çatalhöyük, Turkey in order to understand material loss in walls and buildings, identify potential underlying causes, and create a plan for physical interventions. This paper explains how a multi-temporal laser scanning workflow using the M3C2 method can be leveraged successfully to quantify—with millimeter-level accuracy—the decay of large earthen sites and inform future conservation interventions. This approach allows for the identification of the wall features with the most immediate risk of deterioration based on the detection of patterns of change and calculation of its significance as a preventative measure. Results presented in this paper suggest that the proposed method can be used effectively to enhance site monitoring and perform preventative on-site interventions at large earthen sites earthen sites in the Middle East, Africa, Europe, and the Americas.

Keywords: Çatalhöyük; terrestrial laser scanning; earthen architecture conservation; surface change detection; Multiscale Model to Model Cloud Comparison (M3C2)

1. Introduction

Terrestrial laser scanning (TLS) is a well-established non-contact metric survey technique that delivers high-fidelity three-dimensional (3-D) data of archaeological surfaces and built structures [1,2]. Although archaeologists have employed TLS extensively for stratigraphic and site-wide in-field documentation, site monitoring, and damage assessment [3–14], conservators have employed this technique less frequently to monitor and preserve ancient earthen architecture [15–18]. Despite the high ownership and maintenance costs associated with TLS [19] and the availability of alternative intra-site digital documentation technology [20], laser scanning is still the most feasible option for intra-site documentation of large and complex sites such as Çatalhöyük. TLS delivers long-range high resolution scans that are not affected by surface texture and can be analyzed in real-time for data quality assurance [21,22].

To use and test the potential utility of TLS for the digital monitoring of earthen architecture, TLS data collection was implemented at the Çatalhöyük North Area beginning in the summer 2012 and was repeated annually through the summer 2017. The Multiscale Model to Model Cloud Comparison technique (M3C2) was used to analyze these multi-temporal TLS data [23]. Qualitative data collected by the Çatalhöyük Conservation Team from 2015 to 2017 was also considered alongside quantitative data collected in this research to analyze the series of multi-temporal TLS data and assess the progressive decay and erosion of the North Area buildings. Although previous work in environmental remote sensing used the M3C2 technique to detect complex topographical changes in natural landscapes [24–27], to the best of our knowledge, this paper presents the first systematic attempt to use this method as an archaeological heritage monitoring tool. We argue that this comparative approach is able to identify the wall features most immediately at risk of deterioration and identify and corroborate suspected agents (e.g. water, moisture). It also can inform the creation of a pragmatic and dynamic program for preserving archaeological heritage in compliance with UNESCO periodic reporting guidelines for World Heritage site management [28].

The implementation and testing of the proposed site monitoring approach was driven by a series of research questions that contextualize the usage of TLS for archaeological heritage

conservation and site monitoring. Can the monitoring of earthen architecture sites, such as Çatalhöyük, be enhanced by employing intra-site terrestrial laser scanning surveying and semi-automated analysis of TLS data? How can micro-differences only visible in the 3-D point clouds inform the assessment of employed conservation techniques? Is it viable to use TLS data and surface change detection methods to quantitatively inform site preservation?

2. Research Aim

The aim of this study is to explore the potential utility of multi-temporal 3-D surveying data comparison using the Multiscale Model to Model Cloud Comparison technique method as an archaeological heritage monitoring tool. This study proposes to use this method in the field of earthen architecture conservation and site monitoring to detect material loss in walls and buildings recorded over time by means of terrestrial laser scanning. The main goal is to define a methodology, or workflow, which is able to quantify—with millimeter-level accuracy—the decay of large earthen sites, identify potential underlying causes, and provide conservators and site managers with quantitative information to use for planning physical interventions. It is argued that the proposed workflow allows for creating comprehensive site monitoring programs in compliance with UNESCO periodic reporting guidelines.

3. Research Context

Çatalhöyük is a nine-thousand-year-old Neolithic city (7100-5900 cal BCE) located in the Konya plain in central Anatolia—near the town of Çumra (37° 40’ 19.64’’ N, 32° 49’ 24.63’’ E)—which is considered a key site for understanding human prehistory [29]. The 13.5-hectare East Mound is a very rare, well-preserved example of a Neolithic settlement that grew to a population of about 8,000 people [30]. Researchers with the Çatalhöyük Research Project have identified 18 superimposed building levels documenting the site as one of the earliest fully agricultural and densely populated urban contexts in the Middle East (Fig. 1).

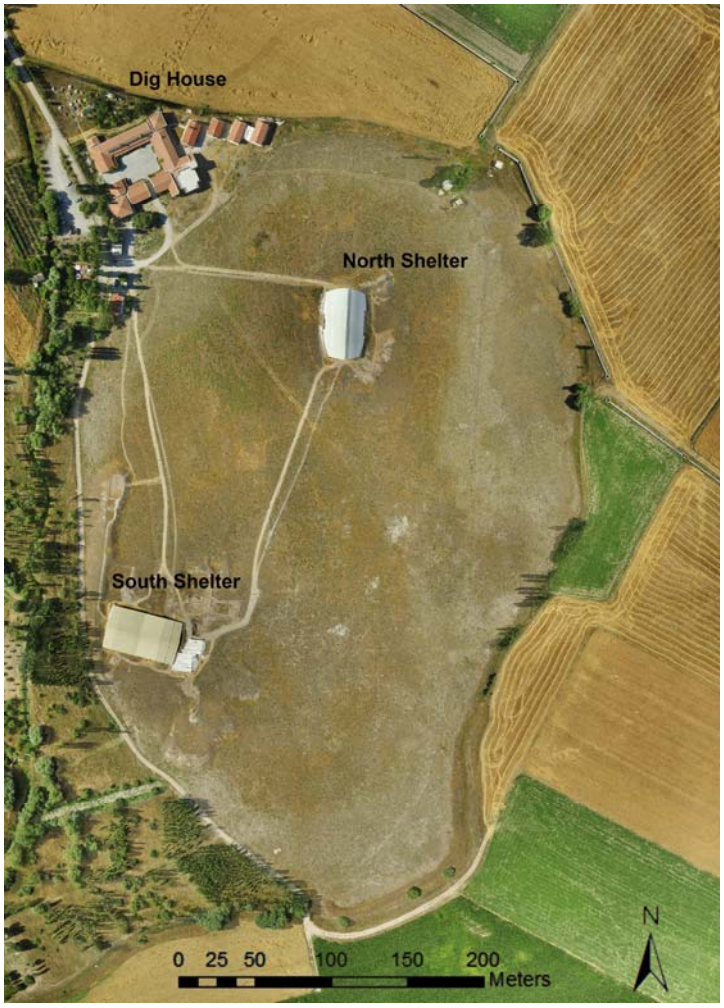

Fig. 1 Aerial Orthophoto of the Çatalhöyük East Mound in July 2015. Source: HIVE Lab

Çatalhöyük is also known for its elaborate art and symbolism, which have allowed researchers to better understand the social and symbolic processes underpinning early village formation, agricultural intensification, and religious ritual [31,32]. The inhabitants of the mound at Çatalhöyük lived in mud brick (adobe) houses that were elaborately overlaid by each successive generation with very similar plans and internal arrangements in an effort to create links between themselves and their past [33].

Çatalhöyük is at-risk because its buildings, composed of fragile mud brick, are constantly threatened by the harsh continental climate of its environment. Due to intensive agricultural practices in the region salinity is increasing [34], which may potentially aggravate damage caused by soluble salts concentrated within the earthen architecture. Even though Çatalhöyük was listed on the UNESCO World Heritage List in 2012, there are still many challenges facing its long-term preservation [35]. Large-scale earthen architecture sites such as Çatalhöyük, are inherently difficult to monitor and conserve. The pathologies that affect its adobe structures are similar to conservation issues recorded at other earthen sites in the Middle East, Africa, Europe, and the Americas [36] (Fig. 2).

Conservators and specialists with the CRAterre-ENSAG Lab and the UNESCO World Heritage Earthen Architecture Programme (WHEAP) [37] observed that about a quarter of the properties inscribed on the UNESCO's List of World Heritage in Danger is made of earthen sites [38]. This remark speaks to the complexity of planning and executing successful conservation interventions on earthen architecture sites, especially as traditional knowledge and methods for maintaining adobe buildings are quickly disappearing and environmental risk is increasing due to rising global temperature [39]. Although Çatalhöyük is not currently included on the List of World Heritage in Danger, once excavated, its earthen architecture is constantly threatened by water, moisture, and adverse environmental conditions.

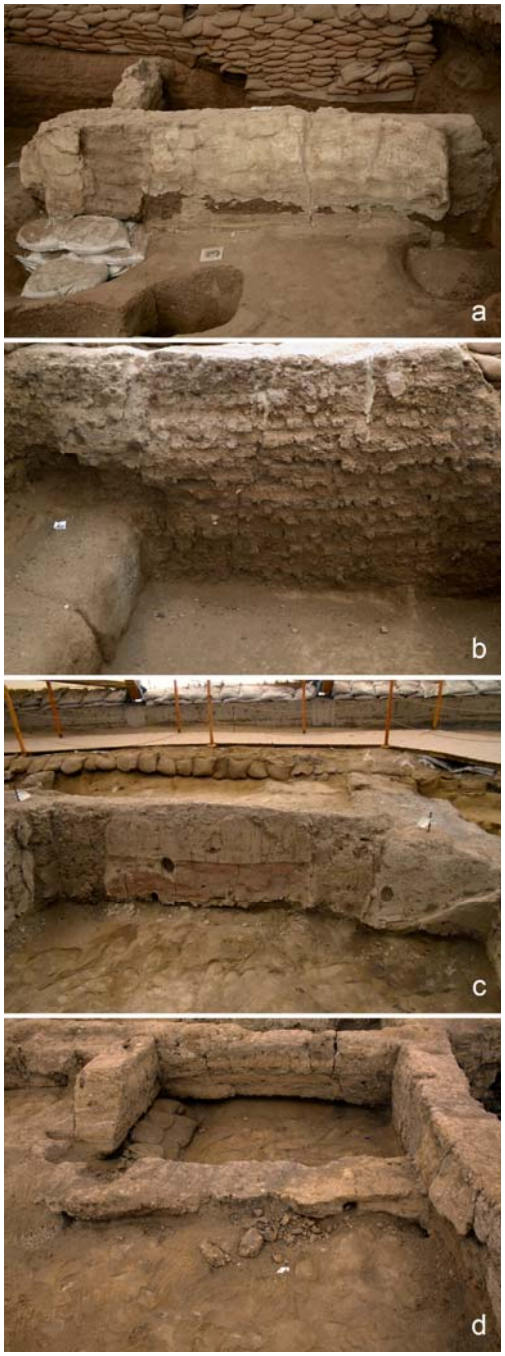

Fig. 2 Conservation issues in the North Area: (a) plaster delamination in F.230 (b) surface erosion in F.225 (c) wall undercutting in F.1617, and (d) collapse in F.2106. Source (a)-(d): Ashley Lingle. Source: HIVE Lab

4. Materials and Methods:

4.1. Properties of Çatalhöyük Earthen Architecture

Previous work on earthen architecture conservation identifies wet/dry and freeze/thaw cycles as the main environmental factors that affect adobe because these processes destabilize the soluble salts concentrated in earthen architecture [36,40–45].

Many years of Çatalhöyük building monitoring have identified water and moisture as major causes of severe *in-situ* conservation issues such as plaster delamination (Fig. 2a) and surface erosion (Fig. 2b), or critical conservation issues including wall undercutting (Fig. 2c) and collapse (Fig. 2d). These threats significantly affect the preservation of walls and other archaeological features in all

excavated areas on the East Mound and compromise the statics of the excavated buildings and vertical sections. As an attempt to mitigate such issues, in 2003, a permanent shelter was built over the South Area. Following the relative success of this shelter, a permanent shelter was also built over the North Area in 2008 to mitigate the conservation threat of direct exposure to water and snow. However, a poorly designed roof vent located at the top of the North Shelter and deteriorated PVC flaps that cover its lower portion expose the earthen structures to water from the east, north, and south (Fig. 3).

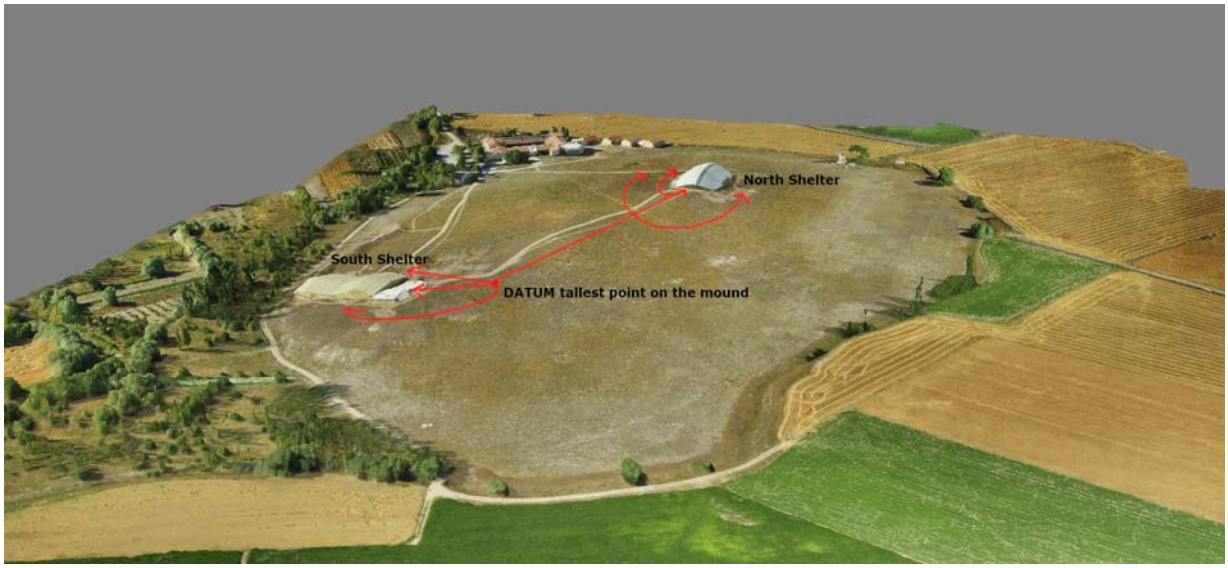

Fig. 3 UAV-based digital photogrammetric 3-D Model of the Çatalhöyük East Mound showing estimated water movements as recorded in November 2015. Source: HIVE Lab and Ashley Lingle

In addition, snow buildup along the west side of the North Shelter further contributes to damage buildings and spaces located along its west edge. Beginning in 2016, sandbags, polythene sheeting, and modifications to the roof flaps were installed to direct water runoff out of the shelter, but additional monitoring and mitigation are needed to prevent water from further damaging the excavated buildings.

An additional conservation threat that causes material loss at the base of Çatalhöyük adobe walls is the capillary action of humidity rising from the ground [35]. When relative humidity is high (RH > 65%), salt deliquescence occurs, and the capillary forces within the mudbrick walls enable water with salt solutes to travel within the adobe structure, leading to sub-florescence. Dissolved salt begins to recrystallize when RH decreases (< 20%), causing considerable internal stresses that fractures and separates the composition of the walls, ultimately resulting in material loss [46].

4.2. Instrument Set Up and Multi-temporal TLS Survey Specifications

TLS point clouds are sets of data points in a 3-D coordinate system defined by X, Y, Z coordinates. They are used in archaeology and heritage conservation to measure the distance between the scanner and external surfaces of stratigraphic units, features, buildings, or artifacts to infer their 3-D morphology for in-field documentation, digital preservation, or site monitoring. TLS point clouds also record information about surface color and the intensity of the laser signal it reflects [47], providing additional information on the texture and material of the scanned object.

A multi-temporal TLS survey is usually employed to measure an archaeological site over time, producing series of historic 3-D data that track changes over a given period. Depending on the temporal frequency of the TLS survey, surface material loss of an excavated building or wall features can be monitored daily, monthly, yearly, decennially, etc. To achieve higher measurement accuracy, it is customary that scanning sessions in this type of surveys are performed using the same laser scanning unit, location of scans, and reference targets, when possible.

Survey Year	Area	No of Scans	∆ No of Scans over prev. year	Res.	Qual.	Point distance (in mm) @10m	No. of pts. in million/ scan	No. of GCPs (Sphere Targets)	Reg. Max. Point Error	Reg. Mean Point Error	Reg. Min. Overlap
2012	North	35	N/A	1/8	4x	12,272	10.9	15	3.3 mm	2.2 mm	61.9 %
2013	North	42	20%	1/8	4x	12,272	10.9	46	14.2 mm	4.1 mm	23.3 %
2014	North	50	20%	1/8	4x	12,272	10.9	38	3.3 mm	1.7 mm	64.7 %
2015	North	51	2%	1/8	4x	12,272	10.9	20	10.4 mm	4.6 mm	21.2 %
2016	North	69	35%	1/8	4x	12,272	10.9	41	8.8 mm	3.4 mm	23.1 %
2017	North	59	-15%	1/5	4x	7,670	28.0	28	5.9 mm	2.8 mm	41.8 %

Table 1 North Area TLS Surveying and Data Processing Specifications

To test the feasibility of using multi-temporal TLS surveying for site monitoring at Çatalhöyük, this study used 3-D data captured yearly in the North Area (Table 1) using a FARO® Focus S120 phase shift laser scanner (Table 2) [48]. As knowledge of the North Area buildings' vulnerabilities and decay increased over the course of this study, the number of scans needed to produce a more and more nuanced 3-D documentation of the case study has increased by a factor of 20% each year between 2012 and 2014 (Table 1). The number of scans recorded in the North Area

remained substantially the same in 2015 over 2014, while it increased again by about 35% in 2016 when the first analytical data from our point cloud comparison became available. Once it became clear that, due to an upcoming change in the management of the site, 2017 would have been the last opportunity for Çatalhöyük to be scanned for a foreseeable period of time, the resolution of the scans recorded during the last year in this survey was increased to allow for an ever more precise representation of the mudbrick buildings' surfaces for preservation purpose (Table 1). To avoid an excess of redundant data in the 2017 survey, the number of scans was accordingly reduced by about 15% over 2016. To compensate for the aforementioned fluctuations in number of scans and subsequent difference in point density during each survey year, upon completion of the data acquisition area-wide point clouds for the North Area were processed in FARO® Scene using filters, such as *Distance Filter* and *Create Project Point Cloud*. The first filter deletes points outside of a maximum distance range set by the user—in this case 10m from the scanner—and the second homogenizes the point density and eliminates duplicate points based on a given search radius. It is argued that this method produced fairly homogenous data to be used in the point cloud comparison and analysis described in the Results section below.

Unit	**Type**	**Output**	**Range**	**Field of View**	**Measurem. Speed**	**Ranging Error**	**Ranging Noise @10m**	**Dual Axis Tilt Comp.**	**Power Consump.**
Range finder	Phase Shift	X, Y, Z, Intensity	0.6-120m indoor or outdoor @ 90% albedo	305° v / 360° h	122,000 / 244,000 / 488,000 / 976,000 pts/sec	±2mm @ 10m and 25m, each @ 90% and 10% albedo	1.2mm @10% albedo – 0.6mm @90% albedo	0.015° (accuracy) ±5° (range)	40W (battery) and 80W (while battery charges)
Unit	**Laser power (cw Ø)**	**Wavelength**	**Beam divergence**	**Beam diam. at exit**	**Unit**	**Type**	**Output**	**Resolution**	**Dynamic color feature**
Optical transmitter	20mW (Laser class 3R)	905nm	Typical 0.19mrad (0.011°)	3.0mm, circular	Color Camera	Coaxial camera	RGB	Up to 70 megapixel color	Brightness automatic adaption

Table 2 FARO® Focus 3D S120 Terrestrial Laser Scanner Specifications

More specifically, the multi-temporal TLS survey presented in this paper focuses on a sample of eight North Area buildings (B5, B48, B49, B55, B64, B82, B114, and B119) that were identified

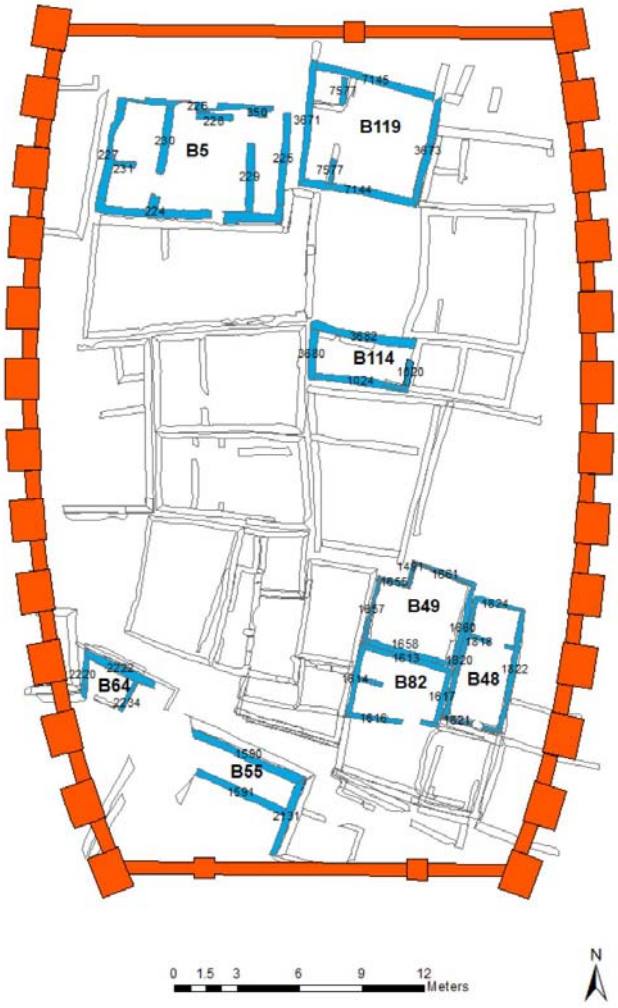

Fig. 4 Map of the North Area. Priority buildings and their features are highlighted. Source: Arianna Campiani

as priority case studies because they were no longer undergoing active excavation, and were managed by Ashley Lingle, the Head of the Çatalhöyük Conservation Team (Fig. 4) and Co-Director of the Çatalhöyük Digital Preservation Project [49], the research framework within which this study was developed.

As discussed in detail in section 4, a set of 39 wall features belonging to those buildings were compared each survey year using the M3C2 plugin in CloudCompare [50,51]. To ensure replicability of the results presented in this paper, all data were archived in an online digital collection allowing open access and free download, including the raw TLS scans captured in the North Area, the related data comparisons performed in CloudCompare, the FARO® Scene data processing projects, and their registration reports and metadata [52].

5. Results

Measuring the distance among identical X, Y, Z points in sets of multi-temporal TLS point clouds allows for surface change to be computed with high precision. This operation quantifies the loss of surface material that occurs in mud brick walls overtime. Alignment using the top-view and cloud to cloud automatic alignment methods in FARO® Scene achieved very high geometric precision, where mean point error was consistently < 5mm per each dataset alignment (Table 1). However, to assess whether the monitoring of earthen architecture at Çatalhöyük can be

enhanced by employing intra-site TLS surveying and semi-automated analysis of TLS data, this study compared pairs of perfectly aligned and identically segmented wall feature point clouds produced in CloudCompare. In all of the wall feature comparisons, references (base clouds) were selected among North Area features scanned in 2014. This choice was driven by the observation that the 2014 raw scans were of optimal quality, their relative area-wide registration error was the lowest of all the available data sets (Table 1), and the 2014 point clouds enabled the evaluation of previous conservation interventions that occurred before the qualitative assessment was conducted in 2015.

Adapting the standard TLS survey and post-processing workflow proposed by Olsen and colleagues to the specificity of our research questions [13], this study designed and field-tested a new multi-temporal TLS survey workflow adding the M3C2 surface change detection method to the analysis phase. To detect surface change in the eight North Area priority buildings using the M3C2 method, each instance of a compared feature (e.g. F230 in 2012, 2013, 2015, 2016, and 2017) was aligned to its reference point cloud (e.g. F230 in 2014). This operation was performed using the 3-Point Registration tool in CloudCompare with the goal of achieving the lowest useful registration error value (RMS). In the M3C2 method, achieving a low RMS value in the registration phase is fundamental to factor in the accuracy of the point cloud

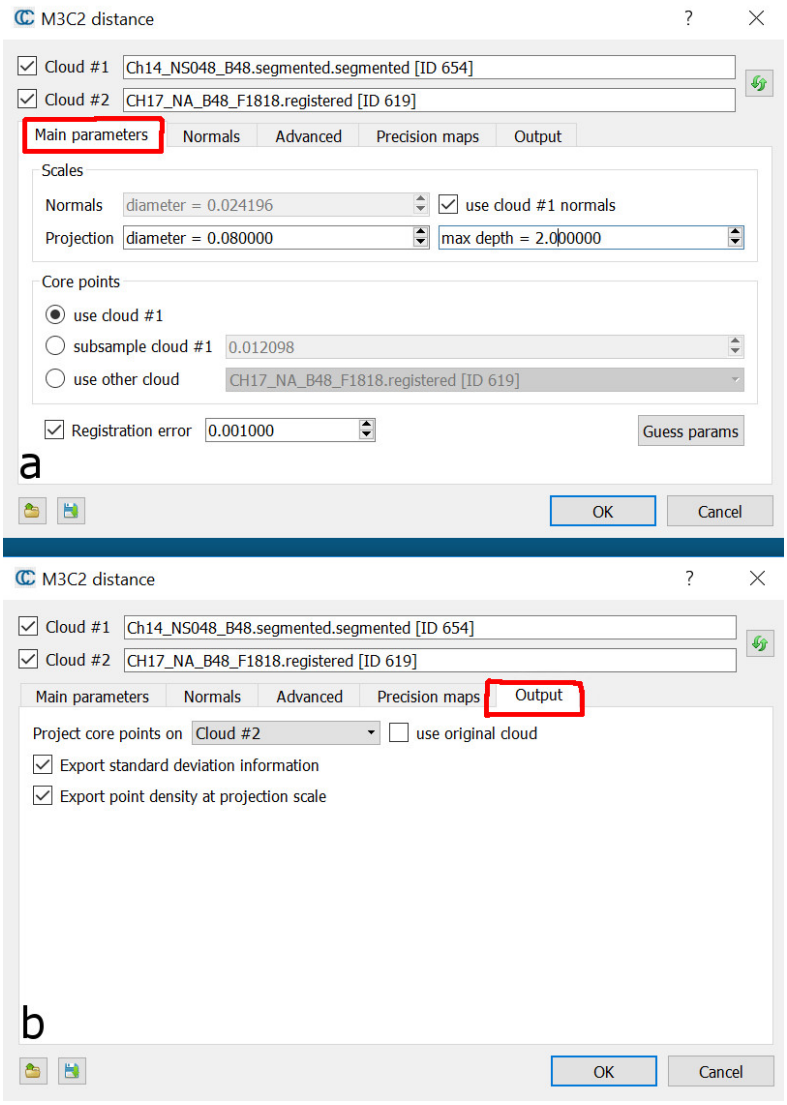

Fig. 5 M3C2 Surface Change Detection parameters used in CloudCompare. Source: Nicola Lercari

alignment [23] and to avoid false positives in the subsequent surface material loss comparison. While computing M3C2 surface change in a pair of point clouds, said RMS value thus needs to be manually entered in the Registration error field per each of the comparisons (Fig. 5).

The following step in the workflow entails computing point normals for the reference cloud to detect change (as point distances) along the normal's direction. To cope with the complex morphology of the compared wall features, our study oriented the normals using the Minimum Spanning Tree method in CloudCompare (Fig. 6) [53].

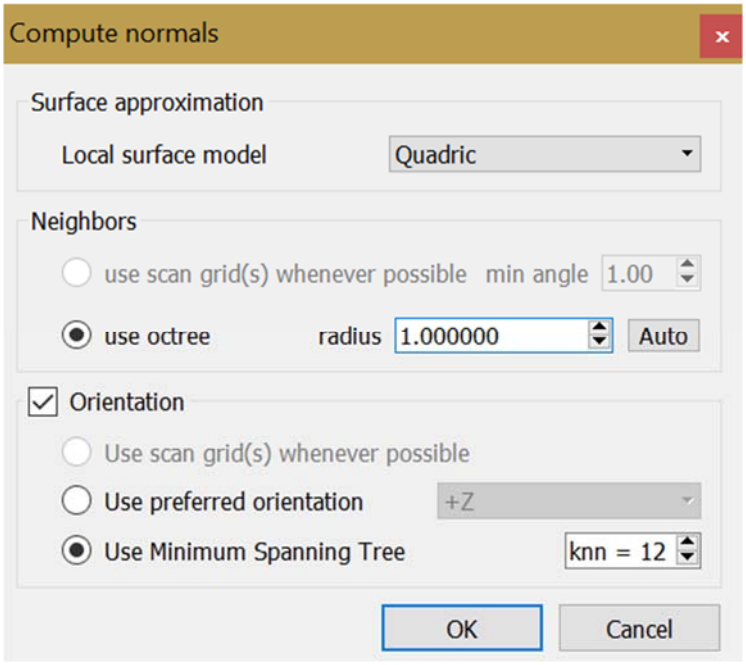

Fig. 6 Surface and normals computation parameters used for M3C2 surface change detection. Source: Nicola Lercari

As compared TLS point clouds may be characterized by different point density and include millions or even billions of points, the M3C2 method usually compares a sub-set of points (defined core points) automatically subsampled via the M3C2 plugin in CloudCompare using a cylindrical projection with user-defined radius and maximum depth. The plugin uses the core points within the cylindrical projection along with their normals' direction to return very precise and weighted comparisons of TLS data. This study made use of a projection with radius value = 0.080m and a depth value = 2m for all of the compared features. To increase the comparison precision, the M3C2 plugin additionally performs automatic point cloud segmentation making sure the two compared data sets have almost identical dimensions. Hence, this semi-automated process decreases the chance of points not having almost identical references in the base cloud, and it avoids mistakenly registered false distance values. More importantly, the M3C2 method returns information on the amount of significant change that has occurred on different portions of a wall feature. The latter value sheds light on whether the point distance values actually correspond to real change or not. This work has successfully leveraged

the M3C2 method to compute and visualize significant change in all of the 39 wall features per each of the five survey years compared to our 2014 reference dataset. All of the M3C2 comparison results were then exported as ASCII format point clouds. Among other data, this format includes significant change, distance uncertainty, and M3C2 distance values for each of the millions of points that were computed in the comparison of two point clouds.

As final step of the proposed workflow, a MATLAB program was created to read said ASCII point clouds and average the computed material loss into a single numeric value per each comparison. [54]. The following high-level pseudocode was created as a reader's guide for non-programmers to understand the functionalities of this MATLAB routine:

1) Load input text file with format:
//X,Y,Z,Npoints_cloud1,Npoints_cloud2,STD_cloud1,STD_cloud2,significant change,distance uncertainty,M3C2 distance,Nx,Ny,Nz
919984
1042.822265625000,1194.622070312500,1010.627746582031,1158.000000,957.000000,0.004416,0.005624,1.000000,0.004358,-0.009361,-0.050169,-0.896264,0.440674
Where the first line is the header, the second line is the number of rows, and the third line is a repeating data series matching the header.
2) Collect all Distance and Certainty fields.
3) Compute points where Distance < Threshold
4) Eject uncertain points where Uncertainty < Calibrated Percentage
5) Transpose data into new file and save.

Readers with a stronger technical background will find more nuanced information on the functionalities of the routine directly in the heavily-commented source code, which is available for download from a repository hosted on GitHub [54].

As discussed by Campiani and colleagues, averaging surface change information—made of millions of M3C2 distance values—in a single parameter has proven extremely useful for expanding the assessment of the TLS monitoring at Çatalhöyük using a GIS platform. For instance, single-digit values representing the surface change in a wall feature can be ingested in the attribute table in GIS to conduct spatial analyses on its related dataset [55,56]. The aforementioned MATLAB program thus averages millions of distance values, describing surface

change in the compared point clouds, then returns a single value. If the distance uncertainty for a compared point is below the threshold, that value is not included in the average. After numerous attempts, an optimal threshold of 0.021 was identified after analyzing the results of several cloud comparisons. For instance, for a threshold of 0.021 there is a certainty of 97.90% that such a point has changed when compared to an almost identical point in the reference cloud. To use this MATLAB program on other datasets, said threshold must be re-calibrated to the sparsity or heterogeneity of the compared point clouds, adjusting its value in increments of ±0.01 to attain proper center.

The results obtained computing surface change detection in all of the 39 North Area wall features included in this study are listed in Table 3. It is argued that archaeologists and conservators working at Çatalhöyük can leverage these results to detect micro-differences in the 3-D point clouds, perform assessments of the state of preservation of surveyed wall features, and evaluate the conservation techniques employed from 2012-2017.

B. No	Feat. No	Area (m2)	Core Pts.	% Significant Change (Significant Change Value / Core Points)					Weighted % Material Loss (Average value / Feature Area)				
				2014 - 2012	2014 - 2013	2014 - 2015	2014 - 2016	2014 - 2017	2012	2013	2015	2016	2017
5	224	9.80	3215885	NA	76.92	78.83	92.14	51.35	NA	0.28	0.12	0.79	0.14
5	225	3.89	3217900	55.22	57.37	71.85	39.30	80.37	0.23	0.04	0.12	0.34	1.67
5	226	7.55	5373560	75.64	80.47	72.74	74.35	51.72	0.27	0.17	0.06	0.28	0.00
5	227	3.09	1560869	NA	78.22	75.00	61.37	92.38	NA	0.12	0.09	0.53	0.29
5	228	0.88	919984	NA	60.31	51.78	43.48	77.24	NA	0.02	0.43	0.44	4.29
5	229	6.87	2619313	NA	41.58	45.74	79.14	38.91	NA	0.06	0.03	0.09	0.04
5	230	7.08	2785921	29.66	53.20	66.26	82.31	67.61	0.07	0.04	0.10	0.05	0.02
5	231	1.85	641450	15.44	50.25	73.53	69.17	39.33	0.00	0.10	0.81	0.08	0.36
5	350	0.30	988277	0.00	50.07	9.42	76.69	NA	0.00	0.31	0.00	4.87	NA
114	1020	1.17	331606	39.24	45.66	62.77	75.73	12.97	0.38	0.63	1.08	0.58	0.00
114	1024	3.73	1214728	NA	57.36	33.67	24.22	66.80	NA	1.14	0.31	0.14	0.05
55	1590	4.04	698136	9.50	9.91	0.41	7.15	15.87	0.39	0.04	0.00	0.10	0.01
55	1591	2.38	467640	66.31	NA	45.39	18.84	70.84	0.56	NA	0.28	0.27	0.33
82	1613	2.25	1200315	24.13	NA	64.57	25.62	45.04	0.01	NA	0.05	0.30	0.04
82	1614	3.23	571691	70.37	NA	68.26	45.47	57.21	0.07	NA	0.15	0.32	0.21
82	1615	2.49	391410	NA	25.37	23.88	12.88	38.04	NA	0.04	0.41	0.17	0.31
82	1616	1.91	1027665	29.22	61.79	42.07	21.83	18.96	0.04	0.13	0.11	0.09	0.29
82	1617	1.46	800455	20.12	72.16	17.68	10.52	15.51	0.14	0.05	0.16	0.23	0.21
49	1491	1.16	324270	39.89	45.40	36.46	5.36	81.90	5.30	4.54	0.42	0.51	4.45
49	1655	1.45	289865	18.24	32.65	80.61	63.60	34.21	0.15	0.50	2.38	0.01	0.12
49	1657	2.85	527078	60.37	28.45	54.91	66.26	80.74	0.09	0.06	0.09	0.08	0.15
49	1658	3.46	1175785	30.35	17.16	89.62	39.30	87.04	0.13	0.05	0.56	0.20	0.16

49	1660	3.18	978634	55.25	74.17	60.75	61.22	13.42	0.00	0.08	0.12	0.06	0.07
49	1661	2.03	622684	56.96	33.92	49.79	74.68	81.89	1.36	1.77	0.20	0.06	0.10
48	1818	1.03	147289	26.79	23.67	58.31	23.50	44.18	0.04	0.05	1.92	0.39	1.70
48	1820	1.68	263317	75.38	34.32	64.13	32.56	55.96	0.28	0.08	0.67	0.03	1.20
48	1821	0.48	121951	38.01	22.50	53.25	21.99	87.15	3.57	0.50	1.61	0.00	13.87
48	1824	0.80	86029	44.69	53.24	4.49	76.88	73.62	0.19	0.52	0.31	1.30	1.11
64	2220	0.52	64875	NA	30.17	12.16	19.06	22.70	NA	5.58	0.15	0.00	0.05
64	2222	0.48	327175	42.81	NA	14.15	22.02	41.64	0.32	NA	2.95	0.38	1.61
64	2234	0.41	68951	39.80	NA	49.96	11.31	11.37	0.08	NA	0.22	0.97	1.39
119	3671	6.34	3817216	NA	NA	70.90	34.58	62.56	NA	NA	0.03	0.33	0.22
119	3673	5.28	2049713	NA	NA	58.73	67.73	10.82	NA	NA	0.06	0.11	0.04
114	3680	1.42	601456	NA	66.43	85.80	30.56	52.54	NA	0.44	0.44	0.63	0.56
114	3682	2.49	904373	48.77	56.55	86.05	30.60	64.98	5.59	4.37	0.09	0.66	0.64
119	7144	6.25	3026954	NA	NA	39.67	82.81	66.44	NA	NA	0.03	0.12	0.06
119	7145	6.80	2360000	NA	NA	37.51	27.45	76.44	NA	NA	0.01	0.04	0.02
119	7577A	2.06	566185	NA	NA	73.63	45.40	42.59	NA	NA	0.34	0.18	0.07
119	7577B	0.88	1223256	NA	NA	80.30	54.94	72.76	NA	NA	0.19	0.38	0.02

Table 3 Percentage of Significant Change and Weighted Material Loss computed in this study. When compared point clouds are too scattered (less than 4 core pts. in the cylindrical projection) for our MATLAB routine to average their % Material Loss, an arbitrary value = 0 is given to Weighted % of material loss

5.1. Discussion

To demonstrate the viability of the workflow presented in section 4, finds related to two North Area features (F.231 and F.7145 – Table 3) will be presented in this section. The M3C2 method enabled high-resolution analysis of two walls producing finds on their conservation state and the success of previous conservation intervention.

Feature 231 is an internal east-west wall in Building 5 (Fig. 4). It is quite thin and runs to the west of external wall Feature 227. Since it was excavated in 1998, F. 231 has been affected by erosion and severe wall undercutting. For these reasons, conservators at the site have treated this wall over the past five years (Fig. 7a1).

The M3C2 surface change detection results for Feature 231 corroborate qualitative observations performed by conservators by quantifying material loss in this wall and providing an insight on its rate of decay and the efficacy of conservation interventions already performed (Fig. 9). For instance, computing surface change for F.231 between 2014-2015 (Fig. 7b1) and 2014-2016 (Fig. 7c1), returns a high % of significant change (SC) value throughout the wall. When added to a low value of % of material loss (ML) detected in the same years for this feature (Fig 8), it can be interpreted that minor material loss occurred in 2014-2016 across the entire surface of the

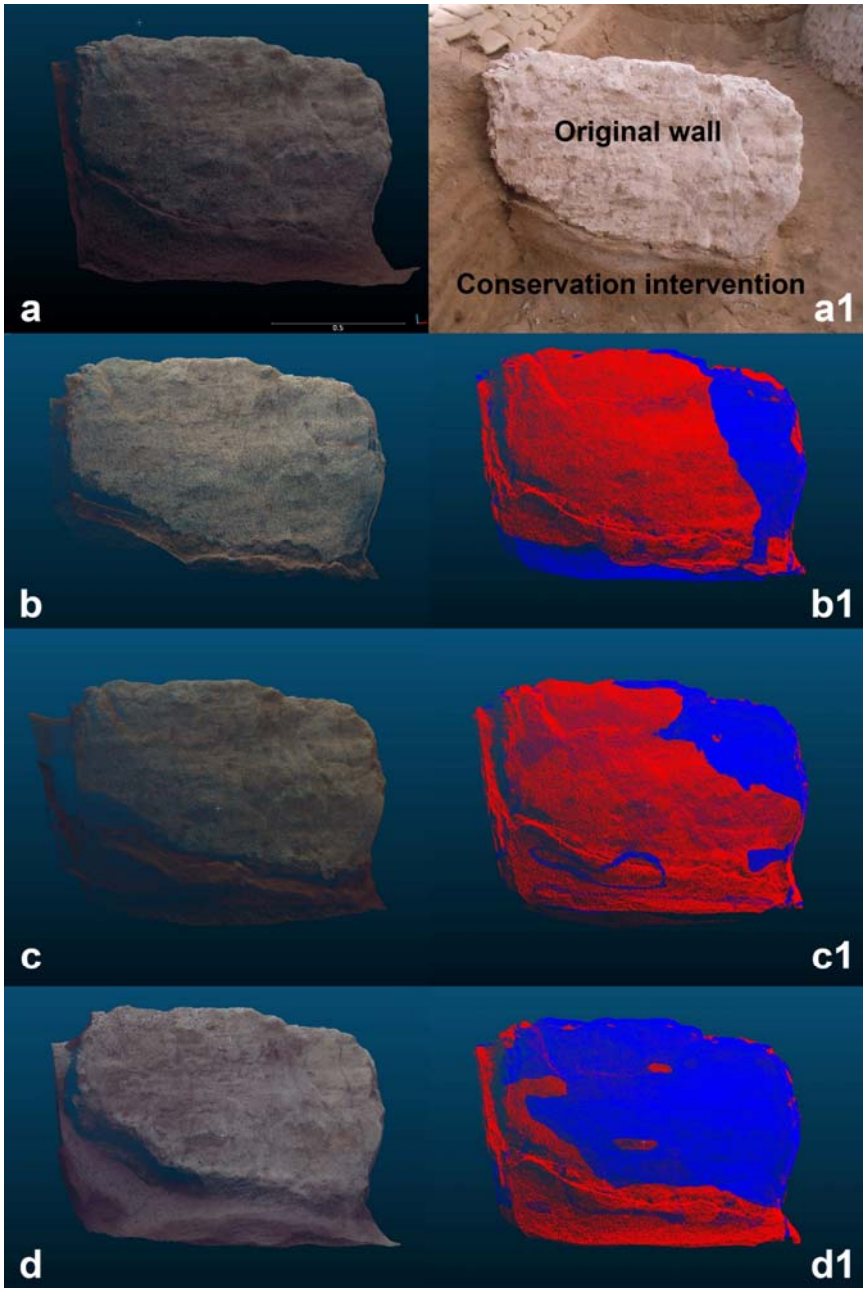

Fig. 7. a) point cloud of F. 231 in 2014 (base cloud); a1) picture of F.231 in 2014; b) point cloud in 2015 and b1) significant change in 2014-2015; c) 2016-point cloud and c1) significant change in 2014-2016; d) 2017-point cloud and d1) significant change in 2014-2017. Significant change is represented by red points (change) and blue points (no change). Source (a1): Ashley Lingle. Source (a, b, c, d, b1, c1, d1): Arianna Campiani and Nicola Lercari

wall. Low % of SC was detected when comparing the feature in 2012-2014 and 2014-2017 (Fig. 7d1). When combined to a low value of % of ML detected in the same years (Fig 8), it can be inferred that minor material loss occurred in 2013 and 2016 only in specific areas of the feature and that conservation interventions conducted in the latter year were successful.

Feature 7145 is the northern perimeter wall of Building 119, which lies next to northern foundation of the permanent shelter covering the North Area (Fig. 4). Excavated in 2013, it has been less affected by conservation issues when compared with other wall features

Fig. 8. % of Significant Change (SC) and % of Material Loss as detected in wall Feature 231 as detected in 2012-2017. High Significant Change > 40%, Low Significant Change < 40%. High % Material Loss > 1.3%, Low % Material Loss < 1.3%. Source: Arianna Campiani and Nicola Lercari

included in this study that were exposed to environmental risk for a longer period. As its excavation occurred after the 2013 TLS survey, no data are available for this feature prior to 2014. Part of F.7145 was covered in well-preserved white plaster that included a geometric wall painting at its eastern edge (Fig. 9a, Fig. 9a1 where painting is covered by sand bags for preservation purpose, and 9b). The M3C2 surface change detection results for F. 7145 in 2014-2015 (Fig. 9b1) and in 2014-2016 (Fig. 9c1) show that the % of SC is low in those years.

When these results are compared with the low values of % of ML (Fig. 10) detected in the same years, it can be inferred that the loss of surface material affecting F.7145 mostly occurred in limited areas around its western and eastern edges and basal area. A high % of SC was detected in this feature between 2014 and 2017 (Fig. 9d1).

Although red areas are predominant in Fig. 9d1, when combined with a low value of % of ML (Fig. 10) detected for the same period, this result indicates minor material loss has occurred only in specific areas of the wall. By analyzing the color information displayed in point cloud of F. 7145 in 2015 (Fig. 9b) and in 2016 (Fig. 9c), it is evident that the geometric wall painting is missing from the latter. This evidence confirms that the proposed surface change detection method is able to determine that such a feature is absent, as it was successfully removed in 2016 by the Çatalhöyük Conservation Team for conservation and display in the Konya Archaeological Museum.

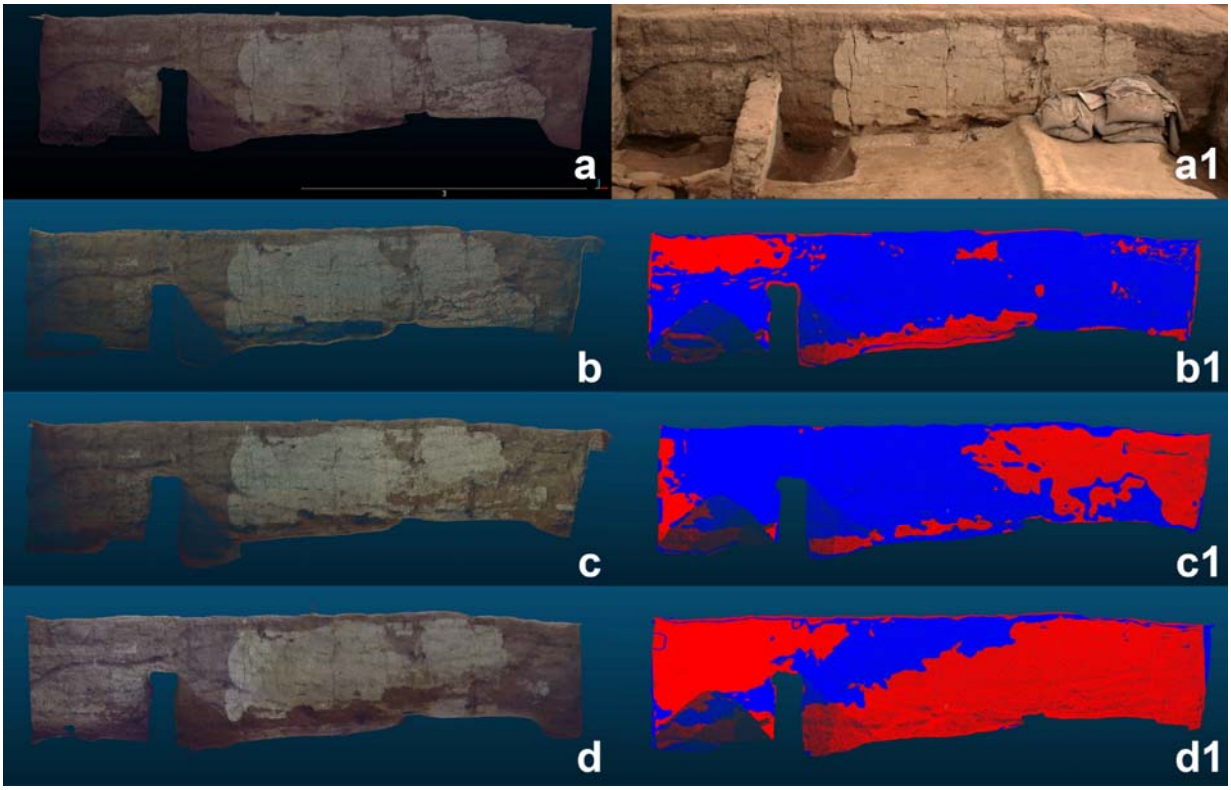

Fig. 9. a) point cloud of F. 7145 in 2014 (base cloud); a1) picture of F.7145 in 2015; b) point cloud in 2015; b1) significant change in 2014-2015; c) 2016-point cloud; c1) significant change in 2014-2016; d) 2017-point cloud; d1) significant change in 2014-2017. Significant change is represented by red points (change) and blue points (no change). Source (a1): Marcin Krzewicki. Source (a, b, c, d, b1, c1, d1): Arianna Campiani and Nicola Lercari

Fig. 10. % of Significant Change (SC) and % of Material Loss as detected in wall Feature 7145 as detected in 2012-2017. High Significant Change > 40%, Low Significant Change < 40%. High % Material Loss > 1.3%, Low % Material Loss < 1.3%. Source: Arianna Campiani and Nicola Lercari

6. Conclusion

This paper discussed the utility of an earthen architecture site monitoring workflow able to compute material loss in mud brick walls over time using multi-temporal terrestrial laser scanning surveying and the M3C2 surface change detection method. It produced high-quality results by comparing about 290 laser scans belonging to 39 external and partition wall features recorded in eight Neolithic buildings in the Çatalhöyük North Area from 2012-2017. This study has proven that the M3C3 method is successful in quantifying surface materials loss in mud brick walls with millimeter-level accuracy, providing conservators and site managers with a powerful tool to detect patterns of change and calculate their significance as a preventative measure. Quantitative information can be exploited to implement data-driven analytical models in GIS for planning conservation interventions and enhance site monitoring strategies [56].

Results presented in this paper demonstrate that a multi-temporal TLS approach has proven to be viable from a technical and methodological standpoint. Significant surface change was detected in all of the eight North Area buildings, documenting, material loss over time in the majority of the 39 wall features analyzed in this study (Table 3). Most significantly, the discussion

of a relevant sample of finds presented in sections 4.1 suggests that the M3C2 method is well suited to detect the magnitude and significance of surface change, providing conservators and site manager with a practical alternative to qualitative assessment. However, there are definite economic/financial limitations, as the adoption of multi-temporal TLS and M3C2 surface change detection can be expensive. This is especially true when the high cost of TLS instrument ownership or leasing for repeated surveys, its operation costs (e.g. annual instrument calibration, warranty extension, import/export documentation, etc.) and personnel costs associated with the lengthy TLS post-processing phase are factored in [19]. A potential solution for utilizing the proposed methods to monitor large sites with limited resources is to adopt alternative surveying technologies, such as Unmanned Aerial Vehicles (UAVs) and digital photogrammetry.

Nevertheless, using a multi-temporal TLS survey approach and M3C2 surface change detection allowed site conservators at Çatalhöyük to get ahead of mudbrick deterioration using a highly-precise preventative measure, in a specific area where said measures are scarcely available. It is thus argued that the proposed method provides a strong basis for quantifying the variance of conservation threats that affect Çatalhöyük by detecting their patterns. Furthermore, these methods can be used to enhance site monitoring and perform preventative on-site interventions at other large earthen sites within Anatolia and beyond that are affected by similar conservation challenges.

Acknowledgments

I would like to thank all of the Çatalhöyük Conservation Team members, in particular: Phil Parkes, and Jerrod Seifert as well as Çatalhöyük Research Project team members Justine Issavi, and Dominik Lukas for contributing to outlining the methods discussed in this article. I also thank UC Merced HIVE Lab students Manuel Dueñas García, Jad Aboulhosn, Moataz Dahabra, Christopher Reps, Estrella García, John Flynn, and Tristan Young for contributing to the data processing, data analysis, and software development. I am particularly thankful to Çatalhöyük Digital Preservation Project Co-Director Ashley M. Lingle and my postdoc Arianna Campiani for being great collaborators and for providing invaluable suggestions on how to design and implement the workflow discussed in this article. I am also grateful to Gina Palefsky for proof reading the manuscript and Ho Jung Yoo and Ryan Johnson for helping curate and publish the data.

Funding

This work was supported by an Archaeological Institute of America Site Preservation Grant and by a University of California President's Catalyst Research Award (Grant ID: CA-16-376911). Funding sources had no involvement in the study design, data collection, analysis, interpretation, nor in the decision to submit the article for publication.

References

[1] J. Mills, D. Andrews, 3D laser scanning for heritage: advice and guidance to users on laser scanning in archaeology and architecture, 2nd ed., Historic England Publishing, Swindon, 2011.

[2] D.D. Andrews, J. Bedford, H. Papworth, English Heritage, Measured and drawn: techniques and practice for the metric survey of historic buildings, English Heritage, Swindon, 2009.

[3] L. Bornaz, F. Rinaudo, P. Ardissone, 3D High accuracy survey and modelling for Cultural Heritage Documentation and Restoration, in: Future Technol. Empower Herit. Prof., Archaeolingua Hun, Brighton, 2007: pp. 19–23. https://www.researchgate.net/publication/235791267_3D_High_accuracy_survey_and_modelling_for_Cultural_Heritage_Documentation_and_Restoration.

[4] J. De Reu, P. De Smedt, D. Herremans, M. Van Meirvenne, P. Laloo, W. De Clercq, On introducing an image-based 3D reconstruction method in archaeological excavation practice, J. Archaeol. Sci. 41 (2014) 251–262. doi:10.1016/j.jas.2013.08.020.

[5] J. De Reu, G. Plets, G. Verhoeven, P. De Smedt, M. Bats, B. Cherretté, W. De Maeyer, J. Deconynck, D. Herremans, P. Laloo, M. Van Meirvenne, W. De Clercq, Towards a three-dimensional cost-effective registration of the archaeological heritage, J. Archaeol. Sci. 40 (2013) 1108–1121. doi:10.1016/j.jas.2012.08.040.

[6] M. Doneus, W. Neubauer, Laser scanners for 3D documentation of stratigraphic excavations, in: E. Baltsavias, A. Gruen, L. Van Gool, M. Pateraki (Eds.), Rec. Model. Vis. Cult. Herit., Taylor & Francis/Balkema, Leiden, 2005: pp. 193–203.

[7] M. Doneus, W. Neubauer, 3D laser scanners on archaeological excavations, in: Proc. XXth Int. Symp. CIPA, Torino, 2005: pp. 226–231.

[8] M. Forte, N. Dell'Unto, K. Jonsson, N. Lercari, Interpretation Process at Çatalhöyük using 3D, in: Ian Hodder, Arkadiusz Marciniak (Eds.), Assem. Çatalhöük, Routledge, New York, 2015: pp. 43–57.

[9] M. Forte, N. Dell'Unto, J. Issavi, L. Onsurez, N. Lercari, 3D archaeology at Çatalhöyük, Int. J. Herit. Digit. Era. 1 (2012) 351–378. doi:10.1260/2047-4970.1.3.351.

[10] G. Landeschi, N. Dell'Unto, K. Lundqvist, D. Ferdani, D.M. Campanaro, A.-M. Leander Touati, 3D-GIS as a platform for visual analysis: Investigating a Pompeian house, J. Archaeol. Sci. 65 (2016) 103–113. doi:10.1016/j.jas.2015.11.002.

[11] T.E. Levy, Cyber-Archaeology and World Cultural Heritage: Insights from the Holy Land, Bull. Am. Acad. Arts Sci. 66 (2013) 26–33.

[12] M. Lezzerini, F. Antonelli, S. Columbu, R. Gadducci, A. Marradi, D. Miriello, L. Parodi, L. Secchiari, A. Lazzeri, Cultural Heritage Documentation and Conservation: Three-Dimensional (3D) Laser Scanning and Geographical Information System (GIS) Techniques for Thematic Mapping of Facade Stonework of St. Nicholas Church (Pisa, Italy), Int. J. Archit. Herit. 10 (2016) 9–19. doi:10.1080/15583058.2014.924605.

[13] M.J. Olsen, F. Kuester, B.J. Chang, T.C. Hutchinson, Terrestrial Laser Scanning-Based Structural Damage Assessment, J. Comput. Civ. Eng. 24 (2010) 264–272. doi:10.1061/(ASCE)CP.1943-5487.0000028.
[14] O. Risbøl, C. Briese, M. Doneus, A. Nesbakken, Monitoring cultural heritage by comparing DEMs derived from historical aerial photographs and airborne laser scanning, J. Cult. Herit. 16 (2015) 202–209. doi:10.1016/j.culher.2014.04.002.
[15] H. Barnard, W.Z. Wendrich, A. Winkels, J.E.M.F. Bos, B.L. Simpson, R.T.J. Cappers, The preservation of exposed mudbrick architecture in Karanis (Kom Aushim), Egypt, J. Field Archaeol. 41 (2016) 84–100. doi:10.1080/00934690.2015.1131109.
[16] J. Barton, 3D Laser Scanning and the Conservation of Earthen Architecture: A Case Study at the UNESCO World Heritage Site Merv, Turkmenistan, World Archaeol. 41 (2009). http://www.jstor.org/stable/40388321.
[17] Y. Fujii, E. Fodde, K. Watanabe, K. Murakami, Digital photogrammetry for the documentation of structural damage in earthen archaeological sites: The case of Ajina Tepa, Tajikistan, Eng. Geol. 105 (2009) 124–133. doi:10.1016/j.enggeo.2008.11.012.
[18] A. Lingle, N. Lercari, A. Campiani, Terrestrial Laser Scanning and Conservation of at-risk World Heritage, in: Society for American Archaeology, Washington, DC, 2018.
[19] N. Lercari, Terrestrial Laser Scanning in the Age of Sensing, in: M. Forte, S. Campana (Eds.), Digit. Methods Remote Sens. Archaeol., 1st ed., Springer International Publishing, 2016: pp. 3–33. http://www.springer.com/us/book/9783319406565 (accessed November 28, 2016).
[20] F. Galeazzi, Towards the definition of best 3D practices in archaeology: Assessing 3D documentation techniques for intra-site data recording, J. Cult. Herit. 17 (2016) 159–169.
[21] F. Fassi, L. Fregonese, S. Ackermann, V. De Troia, Comparison Between Laser Scanning and Automated 3d Modelling Techniques to Reconstruct Complex and Extensive Cultural Heritage Areas, ISPRS - Int. Arch. Photogramm. Remote Sens. Spat. Inf. Sci. XL-5/W1 (2013) 73–80. doi:10.5194/isprsarchives-XL-5-W1-73-2013.
[22] A.P. Spring, C. Peters, T. Minns, Using Mid-Range Laser Scanners to Digitize Cultural-Heritage Sites, IEEE Comput. Graph. Appl. 30 (2010) 15–19. doi:10.1109/MCG.2010.62.
[23] D. Lague, N. Brodu, J. Leroux, Accurate 3D comparison of complex topography with terrestrial laser scanner: Application to the Rangitikei canyon (N-Z), ISPRS J. Photogramm. Remote Sens. 82 (2013) 10–26. doi:10.1016/j.isprsjprs.2013.04.009.
[24] T.B. Barnhart, B.T. Crosby, Comparing Two Methods of Surface Change Detection on an Evolving Thermokarst Using High-Temporal-Frequency Terrestrial Laser Scanning, Selawik River, Alaska, Remote Sens. 5 (2013) 2813–2837. doi:10.3390/rs5062813.
[25] M.R. James, S. Robson, M.W. Smith, 3-D uncertainty-based topographic change detection with structure-from-motion photogrammetry: precision maps for ground control and directly georeferenced surveys, Earth Surf. Process. Landf. 42 (2017) 1769–1788. doi:10.1002/esp.4125.
[26] E. Kleber, E. Nissen, J.R. Arrowsmith, Topographic Change Detection Using CloudCompare Version 1.0, (2013).
[27] R.A. Kromer, A. Abellán, D.J. Hutchinson, M. Lato, T. Edwards, M. Jaboyedoff, A 4D Filtering and Calibration Technique for Small-Scale Point Cloud Change Detection with a Terrestrial Laser Scanner, Remote Sens. 7 (2010). doi:10.3390/rs71013029.
[28] UNESCO World Heritage Centre, Periodic Reporting: A Handbook for Site Managers 2018-2024, (2018). https://whc.unesco.org/en/periodicreporting/ (accessed August 22, 2018).
[29] A. Bayliss, F. Brock, S. Farid, I. Hodder, J. Southon, R.E. Taylor, Getting to the Bottom of It All: A Bayesian Approach to Dating the Start of Çatalhöyük, J. World Prehistory. 28 (2015) 1–26. doi:10.1007/s10963-015-9083-7.
[30] I. Hodder, Women and Men at Çatalhöyük, Sci. Am. 290 (2004) 76–83.

[31] J. Cauvin, Naissance des divinités, naissance de l'agriculture: la révolution des symboles au Néolithique, Cambridge University Press, 1994. https://books.google.com/books?hl=en&lr=&id=UV5q8vHTrxMC&oi=fnd&pg=PR7&dq=naissance+des+divinites&ots=Ion64-HTZP&sig=Vyc769nFwft6VA_GcPrwFB2y18s (accessed August 28, 2016).
[32] I. Hodder, Re-opening Çatalhöyük, in: I. Hodder (Ed.), Surf. Çatalhöük 1993–1995 Çatalhöük Res. Proj. Vol. 1, McDonald Institute for Archaeological Research, Cambridge, 1997.
[33] I. Hodder, The Leopard's Tale: Revealing the Mysteries of Çatalhöyük, Thames & Hudson, London, 2006.
[34] İ. Bahçeci, N. Dinç, A.F. Tarı, A.İ. Ağar, B. Sönmez, Water and salt balance studies, using SaltMod, to improve subsurface drainage design in the Konya–Çumra Plain, Turkey, Agric. Water Manag. 85 (2006) 261–271. doi:10.1016/j.agwat.2006.05.010.
[35] A.M. Lingle, N. Lercari, Çatalhöyük Digital Preservation Project, in: ICOM-CC, Copenhagen, 2017.
[36] L. Rainer, Deterioration and pathology of earthen architecture, Terra Lit. Rev. (2008) 45.
[37] UNESCO World Heritage Centre, World Heritage Earthen Architecture Programme (WHEAP), UNESCO World Herit. Cent. (n.d.). https://whc.unesco.org/en/earthen-architecture/ (accessed August 31, 2018).
[38] David Gandreau, Leticia Delboy, Inventory of World Heritage earthen architecture, (2012).
[39] J. Rogelj, M. den Elzen, N. Höhne, T. Fransen, H. Fekete, H. Winkler, R. Schaeffer, F. Sha, K. Riahi, M. Meinshausen, Paris Agreement climate proposals need a boost to keep warming well below 2 °C, Nature. 534 (2016) 631–639. doi:10.1038/nature18307.
[40] E. Doehne, Salt weathering: a selective review, Geol. Soc. Lond. Spec. Publ. 205 (2002) 51–64.
[41] R. Espinosa, L. Franke, G. Deckelmann, Predicting efflorescence and subflorescences of salts, MRS Online Proc. Libr. Arch. 1047 (2007).
[42] A.S. Goudie, H.A. Viles, Tafoni, alveoles, honeycombs, and overhangs, in salt weathering hazards, Wiley, New York Google Scholar, 1997.
[43] B.V. Ridout, Moisture Monitoring in Earthen Structures, Terra Lit. Rev. (2008) 62.
[44] N. Shahidzadeh-Bonn, J. Desarnaud, F. Bertrand, X. Chateau, D. Bonn, Damage in porous media due to salt crystallization, Phys. Rev. E. 81 (2010) 066110.
[45] F. Uviña Contreras, Adobe architecture conservation handbook, (1998).
[46] F. Matero, E. Moss, Temporary site protection for earthen walls and murals at Çatalhöyük,Turkey, Conserv. Manag. Archaeol. Sites. 6 (2004) 213–227. doi:10.1179/135050304793137694.
[47] K. Tan, W. Zhang, F. Shen, X. Cheng, K. Tan, W. Zhang, F. Shen, X. Cheng, Investigation of TLS Intensity Data and Distance Measurement Errors from Target Specular Reflections, Remote Sens. 10 (2018) 1077. doi:10.3390/rs10071077.
[48] FARO Technologies, Performance Specifications for the Focus3D, FARO® Knowl. Base. (2016). https://knowledge.faro.com/Hardware/3D_Scanners/Focus/Performance_Specifications_for_the_Focus3D (accessed September 12, 2018).
[49] N. Lercari, A. Lingle, O. Umurham, Çatalhöyük Digital Preservation Project_2016, 2016. http://www.catalhoyuk.com/archive_reports/2016.
[50] D. Girardeau-Montaut, CloudCompare, 2019. http://www.cloudcompare.org/ (accessed April 28, 2019).
[51] D. Lague, M3C2 (plugin) - CloudCompareWiki, (n.d.). https://www.cloudcompare.org/doc/wiki/index.php?title=M3C2_(plugin) (accessed September 11, 2018).

[52] A. Campiani, N. Lercari, A.M. Lingle, M. Dahabra, M. Dueñas García, E. García, T. Yang, F. John, C. Reps, Data from: Spatial Analysis and Heritage Conservation: Leveraging 3-D Data and GIS for Monitoring Çatalhöyük Earthen Architecture, (2018). https://doi.org/10.6075/J0WD3XS8.
[53] H. Hoppe, T. DeRose, T. Duchamp, J. McDonald, W. Stuetzle, Surface Reconstruction from Unorganized Points, in: Proc. 19th Annu. Conf. Comput. Graph. Interact. Tech., ACM, New York, NY, USA, 1992: pp. 71–78. doi:10.1145/133994.134011.
[54] M. Dahabra, C. Reps, J. Aboulhosn, M3C2 Material Loss Calculation for MATLAB, (2018). https://github.com/hivelab1/MaterialLoss (accessed October 13, 2018).
[55] A. Campiani, A.M. Lingle, Nicola Lercari, Spatial Analysis and Heritage Conservation: Leveraging 3-D Data and GIS for Monitoring Earthen Architecture, J. Cult. Herit. (2019). doi:10.1016/j.culher.2019.02.011.
[56] A. Campiani, N. Lercari, A. Lingle, Analytical Models for At-Risk Heritage Conservation and 3D GIS, in: Society for American Archaeology, Washington, DC, 2018. http://www.saa.org/Portals/0/SAA/MEETINGS/2018%20Program/Fri.%20Pages%20120-165.pdf.